

Hunting for Brown Dwarfs in the Globular Cluster M4: 2nd epoch HST NIR observations

A. Dieball¹★, L. R. Bedin², C. Knigge³, M. Geffert¹, R. M. Rich⁴, A. Dotter⁵,
H. Richer⁶, D. Zurek⁷

¹*Argelander Institute for Astronomy, University of Bonn, Auf dem Hügel 71, 53121 Bonn, Germany*

²*INAF - Osservatorio Astronomico di Padova, Vicolo dell'Osservatorio 5, I-35122 Padova, Italy*

³*Physics and Astronomy, University of Southampton, SO17 1BJ, UK*

⁴*Department of Physics and Astronomy, University of California at Los Angeles, Los Angeles, CA 90095-1547, USA*

⁵*Harvard-Smithsonian Center for Astrophysics, 60 Garden Street, Cambridge, MA 02138, USA*

⁶*Department of Physics and Astronomy, University of British Columbia, Vancouver, BC, V6T 1Z1, Canada*

⁷*Department of Astrophysics, American Museum of Natural History, New York, NY 10024, USA*

Accepted XXX. Received YYY; in original form ZZZ

ABSTRACT

We present an analysis of the second epoch HST WFC3 *F*110W near-Infrared (NIR) imaging data of the globular cluster M4. The new dataset suggests that one of the previously suggested four brown dwarf candidates in this cluster is indeed a high-probability cluster member. The position of this object in the NIR colour magnitude diagrams (CMDs) is in the white dwarf/brown dwarf area. The source is too faint to be a low-mass main sequence star, but, according to theoretical considerations, also most likely somewhat too bright to be a bona-fide brown dwarf. Since we know that the source is a cluster member, we determined a new optical magnitude estimate at the position the source should have in the optical image. This new estimate places the source closer to the white dwarf sequence in the optical-NIR CMD and suggests that it might be a very cool ($T_{\text{eff}} \leq 4500$ K) white dwarf at the bottom of the white dwarf cooling sequence in M4, or a white dwarf/brown dwarf binary. We cannot entirely exclude the possibility that the source is a very massive, bright brown dwarf, or a very low-mass main sequence star, however, we conclude that we still have not convincingly detected a brown dwarf in a globular cluster, but we expect to be very close to the start of the brown dwarf cooling sequence in this cluster. We also note that the main sequence ends at *F*110W ≈ 22.5 mag in the proper-motion cleaned CMDs, where completeness is still high.

Key words: stars: low-mass – (stars:) brown dwarfs – (stars:) Hertzsprung-Russell and colour-magnitude diagrams – (Galaxy:) globular clusters: individual: M4

1 INTRODUCTION

Brown dwarfs are astronomical objects that are not massive enough to sustain hydrogen fusion. As such, they are “failed” stars, and indeed present a link between planets and stars (Kulkarni 1997). Brown dwarfs were first postulated half a century ago (Kumar 1963; Hayashi & Nakano 1963), but the first detection of a brown dwarf was reported only 30 years later in 1995 (Nakajima et al. 1995; Rebolo et al. 1995). Only in the last decade, large numbers of brown dwarfs have been detected, thanks to increased sensitivities and field of views of modern instruments which enabled large surveys like the Two Micron All Sky Survey (Skrutskie et al. 2006),

the Sloan Digital Sky Survey (SDSS, York et al. 2000), the United Kingdom Infrared Telescope Deep Sky Survey (Lawrence et al. 2007), and the Wide-field Infrared Survey Explorer (Wright et al. 2010). However, due to the intrinsic faintness of these sources, the detection of brown dwarfs is strongly biased towards younger (and hence brighter) and metal-rich brown dwarfs in the solar neighbourhood and in young star clusters or star forming regions (e.g. Casewell et al. 2014; Boudreault & Lodieu 2013). In contrast, we know of only very few old and metal-poor brown dwarfs (and lowest-mass main sequence stars, see e.g. Burgasser et al. 2003, 2009; Lépine et al. 2004; Burgasser et al. 2006; Cushing et al. 2009; Burningham et al. 2014; Troup et al. 2016).

Globular clusters, on the other hand, are among the most metal-poor and oldest stellar aggregates in our Galaxy.

★ E-mail: adieball@astro.uni-bonn.de

They offer the advantage that all members of a globular cluster share the same distance and (to first order) the same age and metallicity - properties that are difficult to obtain for field sources. Because of dynamical evolution, we might expect that most low-mass stars and brown dwarfs would evaporate and be lost to the host globular cluster that have ages of 10 Gyr or more. However, by virtue of their high mass and stellar density, globular clusters potentially host still large numbers of brown dwarfs. This is based not only on their large number of stars but also, stellar interactions might have increased the numbers of brown dwarfs in these systems (e.g. Thies et al. 2010, 2015; Stamatellos et al. 2011; Kaplan et al. 2012).

However, no brown dwarfs have been identified in any globular cluster to date. Since brown dwarfs cannot sustain hydrogen fusion, they become cooler and fainter with time. Thus, we expect that the brown dwarfs in the old Galactic globular clusters are fainter than the lowest mass stars on the main sequence (MS), which sustain their luminosity via hydrogen burning for longer than a Hubble time. Because brown dwarfs in globular clusters have cooled for typically more than 10 Gyr, as a further result of brown dwarf cooling, we indeed expect a gap in the colour-magnitude diagrams (CMDs) of globular clusters between brown dwarfs and the end of the MS. Identifying such faint, sub-stellar objects in globular clusters is therefore challenging and restricts this kind of research to the globular clusters closest to us. The globular cluster M4 (NGC 6121) is one of the closest (≈ 2 kpc, e.g. Bedin et al. 2009) and has been subject to ultra-deep optical studies with the Hubble Space Telescope (HST), see Richer et al. (1997, 2004); Hansen et al. (2004); Bedin et al. (2009) that reach to the bottom of the white dwarf cooling sequence, but just fall short of reaching the end of the MS.

In a previous paper, we reported the detection of four faint sources in the globular cluster M4 (Dieball et al. 2016), based on deep near-infrared (NIR) HST/Wide Field Camera 3 (WFC3) data. Our NIR photometry reaches beyond the expected end of the hydrogen-burning limit toward fainter sources and into the white dwarf/brown dwarf area. Since the white dwarf and the brown dwarf cooling sequence seem to cross in the NIR CMD, we cannot distinguish between white dwarfs and brown dwarfs based on the NIR CMD alone. Archival HST optical data were used for proper-motion cleaning of the CMD and to segregate the white dwarfs from brown dwarf candidates. Since the optical data are not deep enough to detect brown dwarfs, any faint NIR sources lacking optical counterparts are plausible brown dwarf candidates. We found in total four such sources. However, these four sources are only brown dwarf *candidates*, since prior to this study we had no constraint on their membership in the cluster.

In this paper, we present the second epoch NIR HST WFC3 imaging data that are used to proper motion clean all of the first epoch NIR data, and to find cluster members among our brown dwarf candidates. In Sect. 2, we describe the observations and data reduction, followed by an analysis of the results in Sect. 3 and our conclusions in Sect. 4.

2 DATA AND DATA REDUCTION

The observations were obtained with the HST WFC3 IR F110W camera/filter combination for one orbit each on 27th March and 25th July 2017 (program GO-14725, two orbits of F110W imaging, PI: A. Dieball). A total of eight exposures were obtained, each with an exposure time of 653 sec, resulting in a total exposure time of 5224 sec. We observed the same field as in the first NIR epoch (GO-12602, two orbits of F110W imaging and four orbits of F160W imaging), but used a modified four-point WFC3-IRDITHER-BOX-MIN dither pattern and a sampling of NSAMP 14 SPARS 50 to optimise both the sampled point-spread function (PSF) as well as the available exposure time.

A geometrically corrected master image was created based on the pipeline-produced flat-fielded (FLT) images, using *tweakreg* and *astrodrizzle* running under PyRAF (the Python-based interface to IRAF¹). Note that the dithered imaging data allowed us to refine the pixel scale of the master image². This master image serves as reference image to the photometry software DOLPHOT (Dolphin 2000), which runs on the individual flat-fielded images and provides source positions and magnitudes calibrated to the VEGAmag system. We started with the parameter setting that we used for the first NIR epoch data, and then refined some parameters to push our photometry as deep as possible and maximise the detection of faint sources as well as keeping spurious detections somewhat at bay.³ This resulted in 15762 detections, but we caution that these also contain a large number of spurious detections. For more details on the data reduction, creating the master image, and the photometry, see also Dieball et al. (2016).

2.1 Artificial Star Tests

In order to assess the error on the photometry as well as the completeness in our data sets, we carried out artificial star (AS) tests using *dolphot*. We use the same master and input images and parameter setting as in the corresponding original *dolphot* photometry, and rerun DOLPHOT again with the fakesstar parameter set. We expect that not every artificial star will be recovered, which might be due to the artificial source being placed too close to the image edge, or on bad (flagged) pixels, or too close to or on a bright star. Also, the

¹ IRAF (Image Reduction and Analysis Facility) is distributed by the National Astronomy and Optical Observatory, which is operated by AURA, Inc., under cooperative agreement with the National Science Foundation.

² We used *final_scale* = 0.0898 and *final_pixfrac* = 0.9 for the master image.

³ We used *Force1* = 1, *FlagMask* = 4 to eliminate saturated stars, *WFC3IRpsfType* = 1 for the Anderson PSF cores (Anderson 2016), *FitSky* = 2, *SigFind* = 1.5, *SigFindMult* = 0.95, *SigFinal* = 1.5, and *RPSF* = 10, and *Align* = 4 as the reference image has a smaller resolution than the input flat-fielded images. We then selected the DOLPHOT photometry for the following matching and plotting to an object type of no more than 2 (i.e. only “stars”), a sharpness between -0.5 and +0.5, and a crowding of ≤ 0.5 . Note that these selection criteria are less strict than the best-fit selection for the 1st epoch NIR CMD, see Fig. 4 in Dieball et al. (2016). However, we use this approach to push to fainter sources and thus an even deeper photometry.

magnitude DOLPHOT derives is not exactly identical to the input magnitude, which is also expected as environmental effects (blending, crowding, background) impact the derived magnitudes. All these effects are expected to depend on the input magnitude, i.e. a faint star is less likely to be recovered and with a larger deviation from its input magnitude than a bright star. Thus, artificial star experiments are powerful tests of the quality of the photometry.

In order to increase the statistics, a large number of artificial stars should be used. However, this will considerably increase the run time of the AS photometry. Also, since the photometry is performed for each star on each individual input image, the run time also depends on the number of images used. Thus, we ran several sets of AS tests to increase the statistics, but limited the number of stars per run to decrease the run time. For the 2nd epoch of *F110W* observations, which comprised only eight exposures, we used 100,000 artificial stars in total. For the 1st epoch of NIR observations, which consists of eight *F110W* and sixteen *F160W* exposures, we used a smaller number of about 15,000 artificial stars to keep the run time at bay.

Note that we applied the same selection criteria on the artificial source photometry as on the real source photometry, i.e. we allowed only for object type of no more than 2, a sharpness between -0.5 and $+0.5$, and a crowding of ≤ 0.5 . For our error analysis, we use only AS sources that have a magnitude difference of no more than 0.75 magnitudes and are within a 0.5 pixel tolerance radius from the input coordinates. Fig. 1 shows the difference between input and output magnitude versus input magnitude for the selected AS data set.

We divided the magnitude range covered by our AS photometry into bins of one magnitude, and calculated the mean of the differences, determined as $\Delta Mag = \overline{Mag_{in} - Mag_{out}}$, per magnitude bin, plotted as black data points with the corresponding standard deviation as error bars, and listed in Table 1. As can be seen, the mean differences are very small, but their standard deviations increase towards fainter magnitudes. Ideally, the mean difference should be zero, but it becomes larger towards fainter magnitudes, i.e. the recovered magnitude is on average brighter than the input magnitude. This suggests that fainter sources are systematically overestimated and are actually even somewhat fainter than what our photometry derived. In order to correct for this bias, we used the mean differences as fiducial points for a polynomial fit, and applied the obtained correction to all stars in both the AS and the real data photometry. The red data points in Fig. 1 denote the means and standard deviations of the corrected AS photometry, see also Table 1. The correction worked very well for the 1st and 2nd epoch *F110W* data, but we caution that a small offset remained for the faintest magnitude bin that includes only a small number of sources fainter than 26 mag in the *F160W* data. However, this is close to the detection limit anyway, and because the error at this limit is larger than this small offset, we did not attempt further correction.

Most artificial sources were recovered by our DOLPHOT routine. Again, we expect the percentage of artificial sources that are recovered to be magnitude dependent, i.e. fainter sources are less likely to be found and with a larger magnitude error, see above. Fig. 2 shows the percentage of AS sources recovered that fulfil our photometric selection, per

magnitude bin for each filter and epoch. As expected, the completeness drops towards fainter magnitudes and is at 50 % around magnitudes of *F110W*_{2nd} ≈ 24.5 mag, i.e. just around the expected end of the H-burning sequence (see the discussion in Sect.3.3 in Dieball et al. 2016). In the 1st epoch NIR data set, the completeness drops to 50 % around *F110W*_{1st} ≈ 23 mag and *F160W* ≈ 23 mag, about one magnitude above the end of the MS. The difference in completeness between the 1st and 2nd observing epoch is likely due to differences in the sky background and due to different dither patterns used (we used a standard four-point WFC3-IRDITHER-BOX-MIN dither pattern for the first epoch, but modified the dither pattern for the second epoch so that spikes from bright stars are at different positions in the eight exposures).

Whether a source is detected or not depends on its environment, i.e. sky background, crowding and nearby bright stars and their PSF halos and streaks. A faint source is therefore less likely to be detected in the crowded inner parts of a globular cluster - and with a larger photometric error. Thus, we compare the completeness of the entire image (black line in Fig. 2) with the completeness of the area in our master images that is outside a radius of $\approx 2.4'$ from the cluster centre, i.e. the region on the master images outside two core radii (red line in Fig. 2). This area includes all former four brown dwarf candidates. As expected, the completeness in this outer area is somewhat higher at fainter magnitudes and reaches 50 % at *F110W*_{1st} ≈ 24.5 , *F160W* ≈ 24 and *F110W*_{2nd} ≈ 25 mag.

3 THE PROPER MOTION CLEANED CMDS

The 2nd epoch photometry was matched to the first epoch NIR photometry, using 166 known cluster sources with magnitudes $15 \leq F110W \leq 20$ mag that can be clearly identified in both 1st and 2nd epoch master images. The 2nd epoch coordinates were transformed to the 1st epoch image pixel coordinates using the tasks *geomap* and *geoxytran* running under PyRAF. We allowed for up to 2 WFC3 IR pixel matching tolerance between the two epochs. The resulting vector displacement diagrams (VDDs) and the corresponding CMDs are plotted in Figs. 3 and 4. The top panel in Fig. 3 shows the VDDs between the first and second epoch of *F110W* data. Because we used known cluster members for the coordinate transformation, we expect the cluster stars to be located around $\Delta X = 0$ and $\Delta Y = 0$, and indeed we see a tight cluster of data points at that location. A second accumulation of data points can be seen around $\Delta X \approx -0.4$ and $\Delta Y \approx 0.6$, which is mostly due to Galactic bulge stars, see Bedin et al. (2003). The second row of VDDs shows the displacement between the 1st NIR epoch and the optical *F775W* dataset. These VDDs are the same as the VDDs shown in Figs. 5 and 6 in Dieball et al. (2016). The bottom panel shows the corresponding CMDs for sources with *both an optical and a second epoch F110W counterpart*, plus the four brown dwarf candidates (which have no optical counterpart, see Dieball et al. 2016).

We marked our previous four brown dwarf candidates with green (not a cluster member) and red (cluster member) data points, and as can be seen, all four appear in both *F110W* epochs, and hence in the top VDD panel. All magni-

Table 1. Mean differences, $\overline{\Delta Mag} = \overline{Mag_{in}} - \overline{Mag_{out}}$, and standard deviations for all NIR filters and epochs, based on artificial star experiments. Bin sizes are 1 magnitude, and we list the middle of the bin in the first column, followed by the mean differences per magnitude bin in the 2nd epoch *F110W* (2nd column), the 1st epoch *F110W* (3rd column), and the *F160W* data. Only sources with less than 0.75 magnitude difference and that are found within 0.5 pixel tolerance radius of the input coordinates are considered. Lines starting with * denote the mean and standard deviation after photometric correction.

mag	$\overline{\Delta F110_{2nd}} \pm \sigma_{F110_{2nd}}$ [mag]	$\overline{\Delta F110_{1st}} \pm \sigma_{F110_{1st}}$ [mag]	$\overline{\Delta F160} \pm \sigma_{F160}$ [mag]
15.5	0.00 ± 0.02	0.01 ± 0.04	0.01 ± 0.05
*	0.00 ± 0.02	0.00 ± 0.04	0.00 ± 0.05
16.5	0.00 ± 0.02	0.00 ± 0.03	0.01 ± 0.04
*	0.00 ± 0.02	0.00 ± 0.03	0.00 ± 0.04
17.5	0.00 ± 0.03	0.01 ± 0.03	0.02 ± 0.05
*	0.00 ± 0.03	0.00 ± 0.03	0.00 ± 0.05
18.5	0.01 ± 0.03	0.01 ± 0.04	0.02 ± 0.07
*	0.00 ± 0.03	0.00 ± 0.04	0.00 ± 0.07
19.5	0.01 ± 0.04	0.02 ± 0.06	0.02 ± 0.07
*	0.00 ± 0.04	0.00 ± 0.06	0.00 ± 0.07
20.5	0.01 ± 0.05	0.02 ± 0.06	0.03 ± 0.10
*	0.00 ± 0.05	0.00 ± 0.06	0.00 ± 0.10
21.5	0.02 ± 0.07	0.03 ± 0.09	0.05 ± 0.14
*	0.00 ± 0.07	0.00 ± 0.09	0.00 ± 0.14
22.5	0.04 ± 0.09	0.04 ± 0.12	0.06 ± 0.17
*	0.00 ± 0.10	0.00 ± 0.12	0.00 ± 0.17
23.5	0.06 ± 0.13	0.06 ± 0.15	0.07 ± 0.23
*	0.00 ± 0.13	0.00 ± 0.16	0.01 ± 0.24
24.5	0.08 ± 0.18	0.09 ± 0.21	0.07 ± 0.30
*	0.01 ± 0.19	0.00 ± 0.22	0.00 ± 0.30
25.5	0.09 ± 0.26	0.11 ± 0.28	0.08 ± 0.35
*	0.00 ± 0.26	0.00 ± 0.28	0.00 ± 0.37
26.5	0.09 ± 0.30	0.12 ± 0.32	0.23 ± 0.40
*	0.00 ± 0.30	0.00 ± 0.32	0.07 ± 0.52

Table 2. Brown dwarf candidates detected in the first NIR epoch. The second to fifth columns list the magnitudes measured in the first epoch *F110W*, the second epoch *F110W*, and the *F160W* and images, followed by the displacement in the pixel coordinates compared to the first epoch *F110W* master image. The magnitude uncertainties are the errors returned from the DOLPHOT routine.

ID	<i>F110W</i> _{1st} [mag]	<i>F110W</i> _{2nd} [mag]	<i>F160W</i> [mag]	shift pixel
1	24.27±0.02	24.24±0.02	23.39±0.02	0.58
2	25.41±0.05	25.71±0.06	24.75±0.06	0.05
3	24.36±0.02	24.28±0.02	23.60±0.02	0.85
4	26.75±0.16	26.80±0.16	26.13±0.18	1.01

tudes and the displacements for all four brown dwarf candidates are listed in Table 2. Three of the brown dwarf candidates show a displacement larger than 0.1 WFC3 IR pixels, and thus are not considered to be cluster members. Indeed, their location in the VDDs agrees more with field stars. However, our former brown dwarf candidate BD2 shows a displacement of just 0.05 WFC3 IR pixels, which places it in the centre of the VDD that is occupied by cluster members.

3.1 Cluster membership

The position of BD2 in the VDDs, with a displacement of only 0.05 WFC3 IR pixel between the first and second NIR epochs, already suggests that this source is indeed a cluster member.

However, the VDD is also occupied by members of the

Galactic bulge and by field stars. Could BD2 be a member of the field or the bulge population? Fig. 5 shows the CMDs and corresponding VDDs split into seven magnitude bins with widths of 2 mags. Note that we show only sources that are recovered in all three observing epochs: the optical, and the first and the second NIR epochs. The black data points in the CMDs denote sources that show a displacement of no more than 0.1 pixel in *both* sets of VDDs (black data points in the VDDs). Sources with a larger displacement are shown in grey in the VDDs, and sources with a displacement of no more than 0.2 pixel in either set of the VDDs are also plotted as grey data points in the CMDs. The position of BD2 is marked with a red dot in the CMDs.

Interestingly, the bulge population starts to show up only for sources fainter than *F110W* < 17 mag, and recedes again for sources fainter than 25 mag. On the other hand, the cluster sources are prominent throughout the whole magnitude range. We also notice that the distribution of cluster sources fainter than 25 mag is broader, i.e. they show a larger displacement up to 0.3 pixel (but we conservatively only plot sources with a displacement of up to 0.2 pixel as grey data points in the CMDs, see above). Since bulge sources predominantly appear at magnitudes brighter than *F110W* < 25 mag, we might assume that BD2 is not a bulge member.

But how many bulge and field sources can we expect at the position of M 4 in the VDDs, and hence in the CMDs? We use a simplistic approach: To get an estimate for the number of field stars we assume that the distribution of field stars is uniform across the VDD. Thus, we can simply count the number of field stars and scale this number to the area

occupied by the cluster in the VDD. In total, we count 245 sources outside a 0.2 pixel radius centred at 0,0 (i.e. the cluster) and outside a 0.4 pixel radius centred at $-0.35, 0.6$ (the bulge) in the NIR VDD (i.e. top panels in Figs. 3 and 4). We caution that we only consider sources that also have an optical counterpart (black data points). Out of those, only 60 sources are within a magnitude range of $25 < F110W < 26$ mag (the magnitude range in which we find BD2). Scaled to the area of the cluster, we can expect in total 0.6 field sources, and only 0.15 field sources within $25 < F110W < 26$ mag.

If we assume the same for the bulge, we find 464 sources within a circular region centred at $-0.35, 0.6$ and with a radius of 0.4 pixel in the NIR VDD, 23 of those are in the magnitude range $25 < F110W < 26$ mag. Scaled to the cluster, we would expect 29 bulge sources in total, and 1.4 sources with $25 < F110W < 26$ mag. However, the bulge population is clearly not uniformly distributed in the VDD. We assume a normal distribution, and fitting a Gauss function to the bulge distribution in ΔX and ΔY (NIR VDD), we determine a mean (and hence centre of the bulge distribution in the NIR VDD) of $\Delta X = -0.36$ and $\Delta Y = 0.61$, and $\sigma = 0.12$. For sources in the magnitude range of BD2, i.e. $25 < F110W < 26$ mag, the centre of the distribution is slightly shifted and broader at $\Delta X = -0.39$ and $\Delta Y = 0.67$ with a $\sigma = 0.18$. A 0.4 pixel radius corresponds to 3.3σ and encompasses 99.9% of the total bulge population. Thus, only 0.46 sources are expected outside the 0.4 pixel radius. At the position of the cluster and hence BD2 in the VDDs (6σ), the number of bulged sources that can be expected is 4.6×10^{-4} .

We conclude that although it is certainly not impossible that BD2 is a bulge or a field star, it appears very unlikely considering the number of bulge or field sources that are expected in that area in the VDD, especially at such faint magnitudes.

To determine membership probability, we used the method described in Sanders (1971). The method uses two bivariate Gaussian distributions (for field and cluster stars) to fit the measured proper motion distributions in right ascension and declination. From the ratio of the two distributions the probability of the membership can be determined for each proper motion. In order to determine the probability of the source BD2 to be a member of M4, we converted the positional differences shown in Figs. 3 and 4 into proper motions. Only the data from the 1st and 2nd NIR epoch were taken, which provides an epoch difference of 5.1 years (since the source does not appear in the archival optical observations, we could not use the optical data as a further epoch). The VDDs in Figs. 3 and 4 corresponds to the classical vector-point-plot diagram. Since the diagrams in Figs. 3 and 4 show a very clear separation of the cluster and the field stars, we would expect a high probability of BD2 belonging to M4. Our calculations resulted in a membership of more than 99%, which is in good agreement with the results above.

4 DISCUSSION AND CONCLUSIONS

Our NIR observations are designed to push into the brown dwarf region of the CMDs. But is BD2 a brown dwarf? Since we do not have an optical measurement, it is

very difficult to classify this source. Fig. 6 shows the CMDs in all filters for the first and second NIR epochs. Note that we only show sources that have measurements in all epochs, and overplot a 12 Gyr BT-Settl isochrone (red line, Allard et al. 1997, 2013) with a metallicity of $M/H = -1$ dex, and a white dwarf (solid blue line) and a He white dwarf (dashed blue line) cooling sequence⁴ (Holberg & Bergeron 2006; Kowalski & Saumon 2006; Tremblay et al. 2011; Bergeron et al. 2011), all scaled to a distance modulus of 11.2 mag and a reddening $A_V = 1.5$ which gives a reasonably good fit to the underlying data. The errorbars given on the right side of the NIR CMDs are derived from our AS photometry, see Sect. 2.1. We caution again that we could not get a *measurement* for BD2 in the archival optical data. Thus, we show its *previously estimated* position in the optical-NIR CMDs (see Dieball et al. 2016) as a violet triangle, which is on the red side of the bottom of the white dwarf sequence, but on the blue side of the MS, i.e. between the sequences. We had thus classified BD2 as a white dwarf/brown dwarf candidate. Indeed, based on our previous optical estimate, BD2 appears to be too faint and too red to be classified with confidence as a white dwarf, but might just be faint enough to be one of the brightest cluster brown dwarfs, but possibly too blue. However, the location of the brown dwarf sequence in **old and metal-poor** stellar populations is so far unknown. Theoretical considerations (Baraffe et al. 1998; Allard et al. 1997, e.g.) suggest that the brown dwarf sequence turns to the blue and crosses the white dwarf sequence in the NIR. Indeed, this is what we see in the NIR CMDs in Figs. 3 to 6.

But what type of source is BD2?

Could BD2 be a very low-mass MS star? We estimated the end of the H-burning sequence at $F110W \approx 24$ mag. However, the H-burning limit is highly uncertain, see the discussion in Dieball et al. (2016), and depends on the mass of the lowest-mass star that can still support nuclear fusion, which, in turn, depends on the metallicity of the source (see also Fig. 8 in Dieball et al. 2016). Previous theoretical work (e.g. Kumar 1963; Burrows et al. 1993) suggested that the H-burning limit is at higher masses for more metal-poor stars, probably already at $0.09 M_\odot$. If true, this also places the H-burning limit at a brighter magnitude, possibly brighter than our estimate. This agrees nicely with the best-fit NIR CMD presented in Dieball et al. (2016, their Fig. 5), which shows a well populated MS down to $F110W \approx 24$ mag, which then peters out until it crosses the white dwarf sequence around $F110W \leq 25$, when source numbers increase again.

BD2 is at $F110W \approx 25.5$ mag and thus is fainter than our estimated H-burning limit. It seems unlikely that BD2 is a low-mass MS star. However, since this limit is uncertain, if BD2 would indeed be a MS source, it would be the lowest-mass MS star ever detected in a globular cluster to date. If true, this would seriously challenge our understanding of the H-burning limit, as it would imply that the lowest-mass stars that can still sustain hydrogen burning in old (> 10

⁴ The white dwarf cooling sequences were kindly provided by Pierre Bergeron in the HST WFC3 IR filters. We assumed white dwarf masses of $0.5 M_\odot$. See (<http://www.astro.umontreal.ca/bergeron/CoolingModels>).

Gyr) populations would be fainter and at lower masses than previously thought.

Could BD2 be a brown dwarf? We consider it unlikely that BD2 is a MS source, because it is fainter than the expected end of the H-burning MS. But is BD2 a brown dwarf? Brown dwarfs cannot sustain H burning, and as a result, they become cooler and fainter with time. [Caiazzo et al. \(2017\)](#) presented MESA models for 11 to 13 Gyr old stellar populations, and predict a gap between the end of the MS and the beginning of the brown dwarf cooling sequence. For a 12 Gyr cluster, [Caiazzo et al. \(2017\)](#) predicts this gap to be 3 magnitudes wide (see their Fig. 3 and Sect. 4). However, these calculations were done for solar metallicity and in the NIR filters of the James Webb Space Telescope. As discussed above, the metallicity has an impact on the faint end of the H-burning sequence, and likely on the shape and the start of the brown dwarf cooling sequence. In a metal-poor cluster with an age of ≈ 12 Gyr, like M4, the start of the brown dwarf cooling sequence is predicted to be at $F110W = 26$ mag and fainter ([Caiazzo, private communication](#)). Thus, [Caiazzo et al. \(2017\)](#) theoretical considerations seem to suggest that BD2 might be too bright to be a bona fide brown dwarf.

Could BD2 be a white dwarf? Since the white dwarf and brown dwarf cooling sequences cross in the NIR, it is not possible to distinguish white dwarfs from brown dwarfs based on the NIR CMD alone, not even after removing field objects via proper motions. An optical counterpart to BD2 could not be measured, however, a very faint smudge can be seen in the optical master image at the position of BD2. The coolest white dwarfs in M4 have temperatures around 4000K ([Bedin et al. 2009](#)), just below the blue hook (see Fig. 6). Based on our previous optical estimate, BD2 appears fainter and redder than the blue hook at the bottom of the white dwarf cooling sequence (usually seen as the endpoint of the white dwarf cooling sequence) (although it might still be consistent with the white dwarf sequence considering the large errors at such faint magnitudes). However, we now know that BD2 is a cluster member, which allows us to do better on the optical estimate: We worked out the position BD2 would have in the optical image if it would not have moved with respect to the other cluster members. This might introduce a very small error, as also cluster stars do move, but since the change in position is expected to be less than 0.1 WFC3 pixel, we expect this error to be small indeed. Next, we run aperture photometry using DAOPHOT ([Stetson 1987](#)) on all known source positions in the optical master image, and compared the aperture photometry to the PSF-fitting photometry to work out the offset between these two types of photometry, see Fig. 7. This step is necessary because PSF-fitting photometry does not work on the position of BD2 in the optical image as the source signal, if any, is too faint. As can be seen, the spread between the aperture and PSF-fitting photometry becomes larger for fainter sources. Based on this, we now estimate the optical magnitude of BD2 at $F110W \approx 27 \pm 1$ mag. Note the large uncertainty on this estimate. Indeed we find faint sources whose aperture-based estimate deviates by more than 2 magnitudes from the PSF-fitting measurement. We marked the position of BD2 based on the *new optical estimate* with a red cross in Fig. 6. Our new estimate places BD2 closer to the blue hook on the white dwarf sequence in the optical-NIR

CMDs. Based on this, we conclude that BD2 is likely one of the optically faintest and coolest white dwarfs detected in this cluster. BD2's NIR colour and $F110W$ magnitude suggest $T_{\text{eff}} \leq 4500$ K for a white dwarf with a pure hydrogen atmosphere, or $T_{\text{eff}} \leq 2750$ K for a He white dwarf.

We conclude that BD2 is a high-probability cluster member, and, based on the information that we have gathered so far, is most likely not a single brown dwarf but rather a white dwarf. BD2 could well be an exotic source like a He white dwarf (see Fig. 6), or a binary system consisting of both a (He) white dwarf and a bright and massive brown dwarf which might explain its red colour compared to single faint white dwarfs. The source is too faint to be a bona-fide MS star, and likely too bright (and hence too blue in the optical-NIR colour) to be a bona-fide brown dwarf. However, we still caution that we cannot strictly exclude the possibility that BD2 is in fact a very low-mass MS star - and if so, the faintest, coolest and lowest-mass MS star ever detected in a globular cluster to date, or a very bright and massive brown dwarf.

Future NIR observations that include medium wavebands like F127M and F139M might help to distinguish white dwarfs from brown dwarf candidates. This is because the spectral energy distributions (SEDs) of brown dwarfs is governed by molecular absorption of H_2O in the IR, which shifts flux to the NIR wavebands (e.g. [Allard et al. 1997](#)), whereas we expect the SED of white dwarfs to be mostly flat.

We also note the sharp drop in the luminosity function of the MS at $F110W \approx 22.5$ mag. The proper-motion cleaned CMDs in Figs. 3, 4, 5 and 6 suggest that the MS ends around $F110W \approx 22.5$ mag and $F110W - F160W \approx 1$ mag where the completeness is still high at these magnitudes (around 70% (entire field) and 80% (outer region) in the second $F110W$ epoch, and around 60% to 70% (entire field) and 70% to 80% (outer region) in the first NIR epoch, see Fig. 2), and the magnitude uncertainty is only around a tenth of a magnitude. This result might put important constraints on theoretical models on star formation and evolution.

ACKNOWLEDGEMENTS

AD acknowledges support from the German Federal Ministry of Economics and Technology (BMW) provided through DLR under project 50 OR 1707. We thank Pierre Bergeron for providing the white dwarf models (<http://www.astro.umontreal.ca/bergeron/CoolingModels>) in the WFC3 IR filters, and Ingo Thiess and Ilaria Caiazzo for useful discussions. RMR acknowledges financial support from grants GO-14711 and 14725 from NASA through the Space Telescope Science Institute.

REFERENCES

- Alessi, M. & Pudritz, R. E. 2018, MNRAS accepted
- Allard, F., Hauschildt, P. H., Alexander, D. R. & Starrfield, S. 1997, ARA&A, 35, 137
- Allard, F., Homeier, D., Freytag, B., Schaffenberger, W. & Rajpurohit, A. S. 2013, MSAIS, 24, 128
- Anderson, J. 2016, Instrument Science Report WFC3 2016-12, Empirical Models for the WFC3/IR PSF

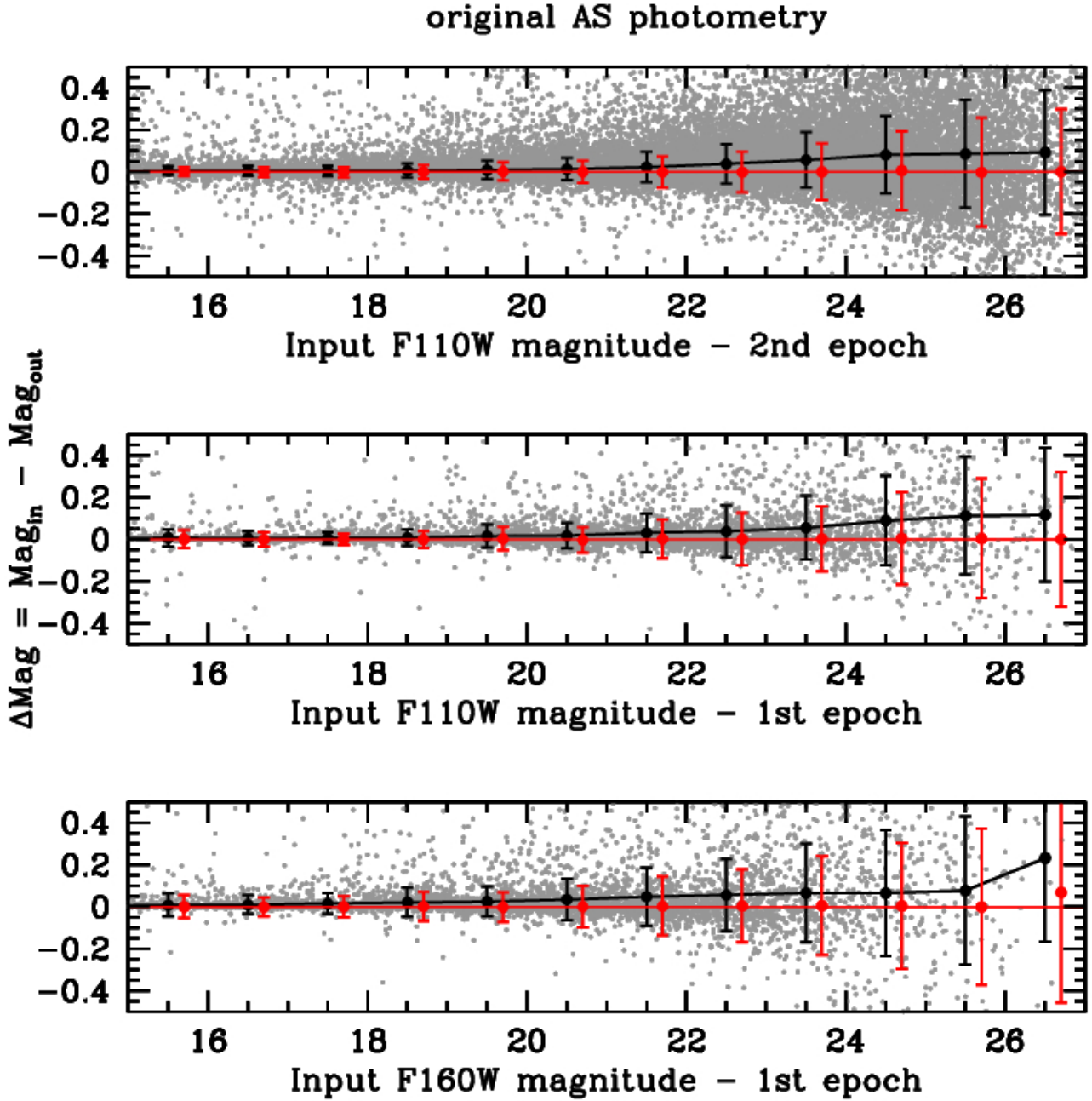


Figure 1. Difference between input and obtained magnitude for artificial stars (dark grey data points). The photometries were performed using *dolphot* and the same parameter set as the respective original photometry. The data points with error bars denote the mean differences $\Delta\text{Mag} = \text{Mag}_{\text{in}} - \text{Mag}_{\text{out}}$ and their standard deviations per magnitude bin for the 2nd epoch *F110W* data (top panel), the 1st epoch *F110W* (middle panel), and the *F160W* data (bottom panel). A clear offset towards fainter magnitudes can be seen in all filters and all epochs. Note that we only include artificial sources within a 0.5 pixel tolerance radius from the input coordinates and within 0.75 magnitude difference. The red data points and error bars denote the mean and corresponding standard deviations after photometric correction. To guide the eye, we have marked $\Delta\text{Mag} = 0$ with a red line. See the text for more details.

Baraffe, I., Chabrier, G., Allard, F. & Hauschildt, P. H. 1998, *A&A*, 337, 403
 Bedin, L. R., Piotto, G., King, I. R. & Anderson, J. 2003, *AJ*, 126, 247
 Bedin, L. R., Salaris, M., Piotto, G. et al. 2009, *ApJ*, 697, 965
 Bergeron et al. 2011, *ApJ*, 737, 28
 Boudreault, S. & Lodieu, N. 2013, *MNRAS*, 434, 142

Burgasser, A. J., Kirkpatrick, J. D., Burrows, A. et al. 2003, *ApJ*, 592, 1186
 Burgasser, A. J. & Kirkpatrick, J. D. 2006, *ApJ*, 645, 1485
 Burgasser, A. J., Witte, S., Helling, C. et al. 2009, *ApJ*, 697, 148
 Burningham, B., Smith, L., Cardoso, C. V. et al. 2014, *MNRAS*, 440, 359
 Burrows, A., Hubbard, W. B., Saumon, D. & Lunine, J. I. 1993,

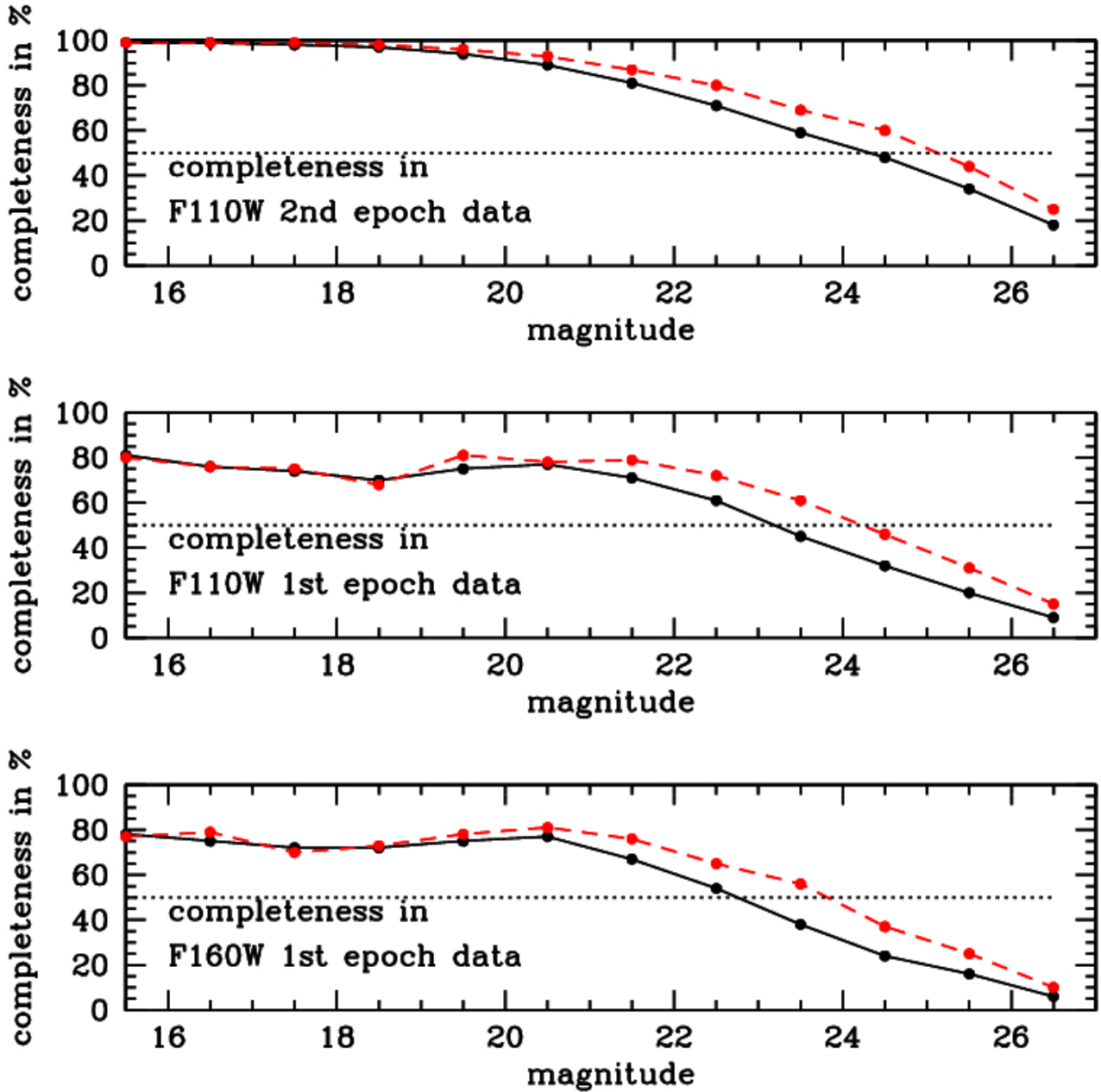


Figure 2. Completeness in % based on artificial star tests. The bottom panel shows the completeness in the (only available) first epoch *F160W* data, the middle of the first epoch *F110W* data, and the top panel of the second epoch *F110W* data. We distinguish between the completeness in the entire master image (black line) and completeness outside a $\approx 2.4'$ radius around the cluster centre that contains all four brown dwarf candidates (red dashed line). As expected, the completeness for fainter sources (fainter than 22 mag) is somewhat higher outside the $\approx 2.4'$ radius because this area is less crowded and contains fewer bright stars. See the text for more details.

ApJ, 406, 158
 Caiazzo, I., Heyl, J. S., Richer, H. & Kalirai, J. 2017, arXiv:1702.0009
 Casewell, S. L., Littlefair, S. P., Burleigh, M. R. & Roy, M. 2014, MNRAS, 441, 2644
 Cushing, M. C., Looper, D., Burgasser, A. J. et al. 2009, ApJ, 696, 986
 Dieball, A., Bedin, L. R., Knigge, C. et al. 2016, ApJ, 817, 48
 Dolphin, A. E. 2000, PASP, 112, 1383

Girven, J., Gänsicke, B. T., Steeghs, D. & Koester, D. 2011, MNRAS, 417, 1210
 Hansen, B. M. S., Richer, H. B., Fahlman, G. G. et al. 2004, ApJS, 155, 551
 Holberg, J. B. & Bergeron, P. 2006, AJ, 132, 1221
 Hayashi, C. & Nakano, T. 1963, Progress of Theoretical Physics, 30, 460
 Kaplan, M., Stramattelos, D. & Whitworth, A. P. 2012, Ap&SS, 341, 395

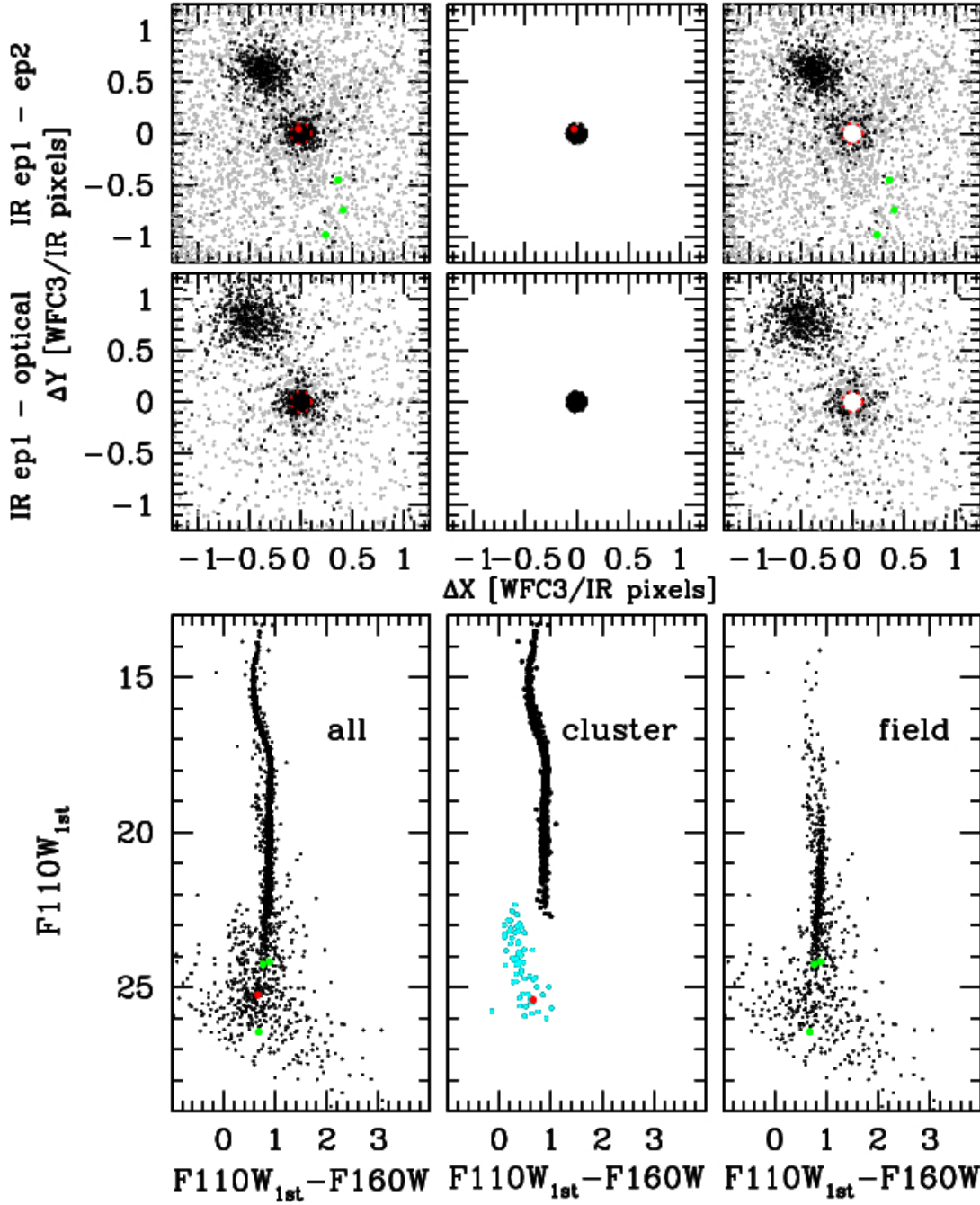


Figure 3. Top row: Vector displacement diagrams (VDDs) between the 1st and 2nd NIR observing epochs. Middle row: VDDs between the optical and the 1st NIR data. Sources that appear in *all* observing epochs are plotted in black, sources that appear only in the corresponding VDD are plotted in grey. Bottom row: The resulting NIR CMDs. From left to right: all data; only sources that have a displacement of less than 0.1 WFC3 pixel in all VDDs which suggests that the sources are cluster members; the remaining field sources that have displacements larger than 0.1 WFC3 IR pixel. The white dwarfs are selected from the optical-NIR CMDs (see [Dieball et al. 2016](#)) and are plotted in cyan. Note that in the CMDs we plot 1st epoch NIR data only, but only sources that also have a counterpart in the second $F110W$ observing epoch, i.e. sources that appear in the optical, the first and the second $F110W$ observing epochs (black data points in the VDDs). We also add the previously reported brown dwarf candidates, plotted in green, if their displacement agrees with being a field source, or in red, if the displacement is less than 0.1 WFC3 IR pixel.

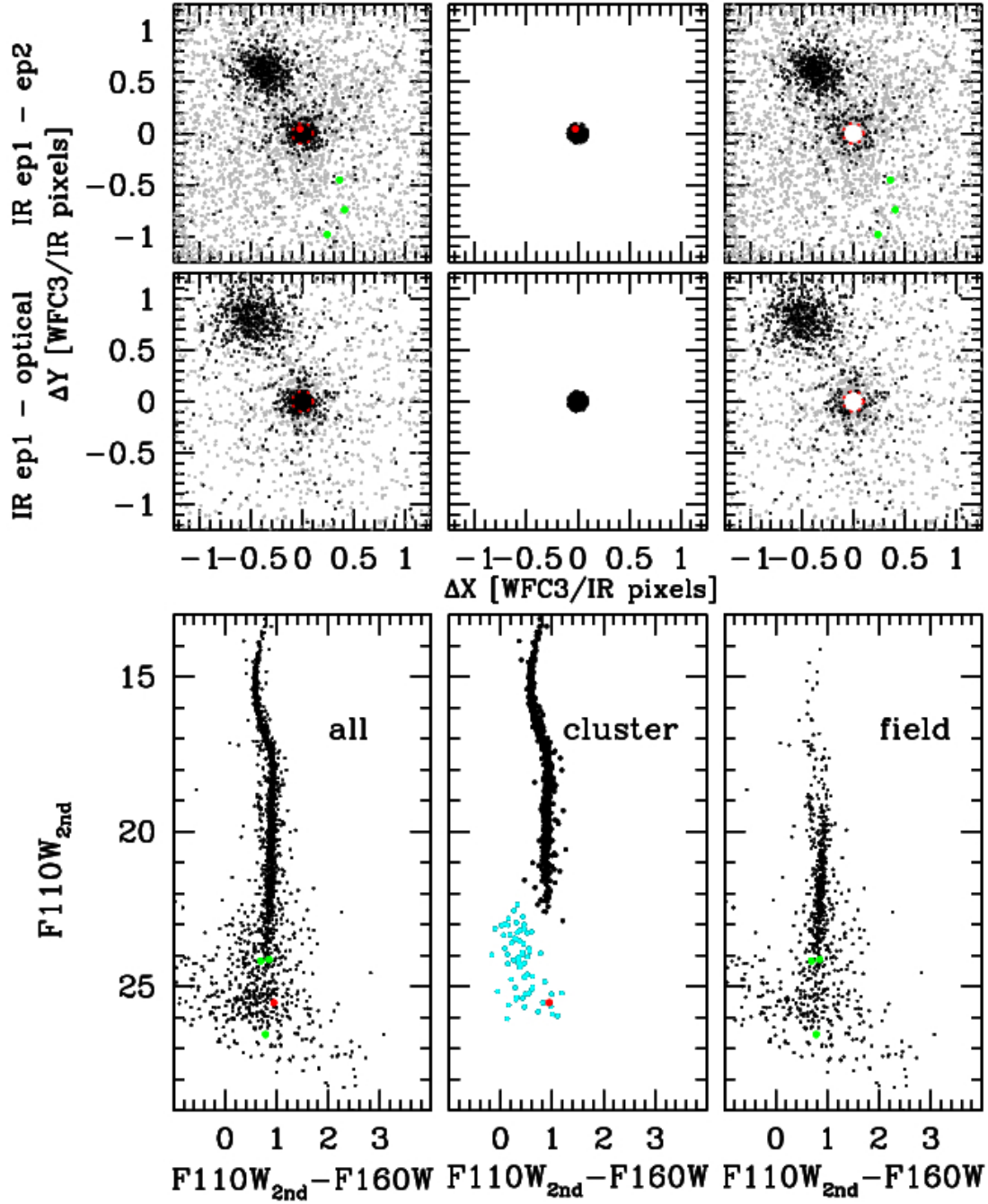


Figure 4. Same as Fig. 3, but the CMDs show the second epoch $F110W$ data against the $F160W$ data. (For the latter, we only have a first epoch, no second epoch of $F160W$ data were obtained.)

Kowalski & Saumon 2006, ApJ, 651, L137
 Kulkarni, S. R. 1997, Science, 276, 1350
 Kumar, S. S. 1963, ApJ 187, 1123
 Lawrence, A., Warren, S. J., Almaini, O. et al. 2007, MNRAS, 379, 1599
 Lépine, S., Shara, M. M. & Rich, R. M. 2004, ApJ, 602, 125
 Nakajima, T., Oppenheimer, B. R., Kulkarni, S. R., Golimowski, D. A., Matthews, K. et al. 1995, Nature, 378, 463
 Rebolo, R., Zapatero Osorio, M. R. & Martín, E. L. 1995, Nature, 377, 129
 Richer, H. B., Fahlman, G. G., Ibata, R. A. et al. 1997, ApJ, 484,

741
 Richer, H. B., Ibata, R., Fahlman, G. G. & Huber, M. 2003, ApJL, 597, 45
 Richer, H. B., Fahlman, G. G., Brewer, J. et al. 2004, AJ, 127, 2771
 Sanders, W. L. 1971, A&A, 14, 226
 Skrutskie, M., Cutri, R. M., Stiening, R. et al. 2006 AJ 131 1163
 Stamatellos, D., Maury, A., Whitworth, A. & André, P. 2011, MNRAS, 413, 1787
 Stetson P. B. 1987, BAAS, 19, 745
 Thies, I., Kroupa, P., Goodwin, S., Stamatellos, D. & Whitworth,

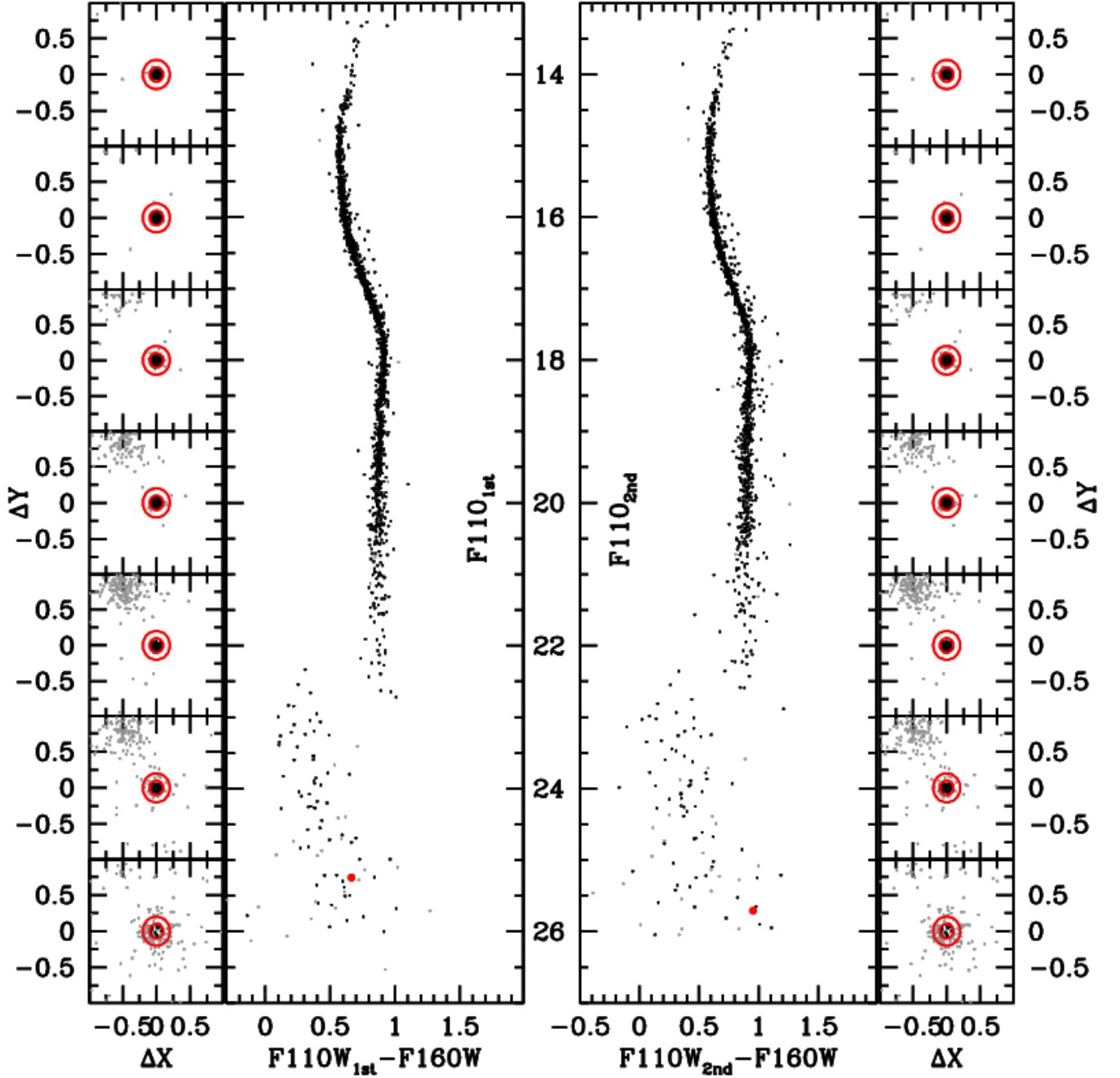


Figure 5. CMDs and corresponding VDDs (outer left and outer right panels), for the 1st epoch NIR data (first two panels), and the second epoch NIR data (last two panels, from left to right). We show the VDDs for sources in magnitude bins of 2 mags in $F110_{st}$ and $F110_{2nd}$. The sources marked in black in the VDDs are only cluster sources, i.e. sources that show a displacement of less than 0.1 pixel between the epochs. Note that we only show sources that are recovered in *all* three epochs: the optical, the first and second NIR epoch. Grey data points in the CMDs denote sources that have a displacement between 0.1 and 0.2 pixel, i.e. sources located in the red annulus in the VDDs. BD2, which has no optical counterpart, is marked with a red data point. See the text for details.

A. 2010, ApJ, 717, 577
 Thies, I., Pflamm-Altenburg, J., Kroupa, P. & Marks, M. 2015, ApJ, 800, 72
 Tremblay et al. 2011, ApJ, 730, 128
 Troup, N. W., Nidever, D. L., De Lee, N. et al. 2016, AJ, 151, 85
 York, D. G., Adelman, J., Anderson, J. E. et al. 2000, AJ, 120, 1579
 Wright, E. L., Eisenhardt, P. R. M., Mainzer, A. K. et al. 2010,

AJ, 140, 1868

This paper has been typeset from a \LaTeX file prepared by the author.

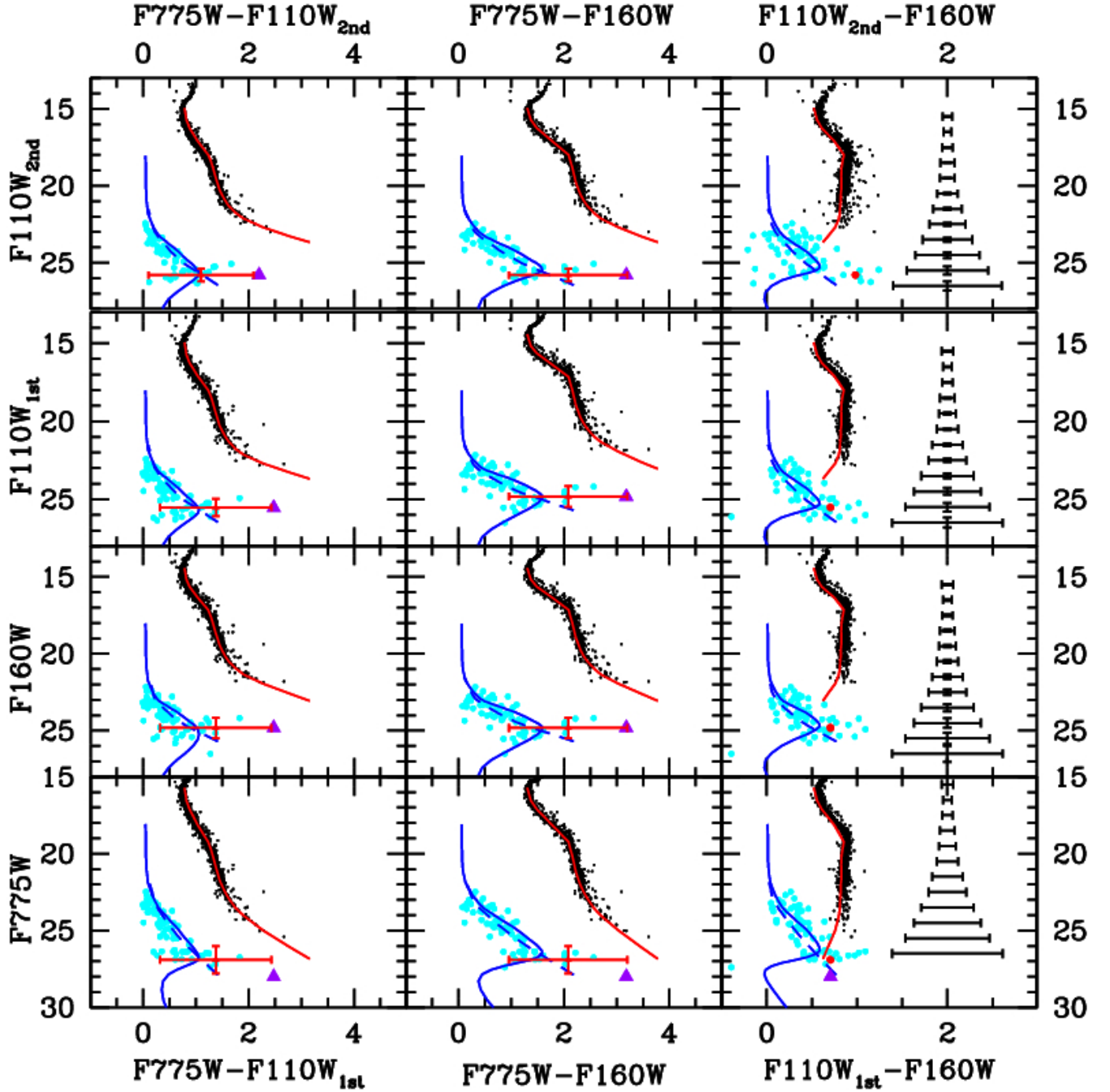


Figure 6. CMDs in all filters and all epochs, we only show sources that have a displacement of no more than 0.1 WFC3 pixel between the optical, the first and the second NIR observing epochs, which suggests that they are cluster members. The blue solid line denotes a white dwarf cooling sequences (for masses of $0.5 M_{\odot}$), the blue dashed line a He white dwarf cooling sequence, and the red solid line a 12 Gyr BT-Settl isochrone. All models fit the underlying data well. Mean photometric errors have been obtained using AS tests and are plotted on the right side of the NIR CMDs, see also Fig. 1 and Sect. 2.1. Note that the mean error was determined for 1 mag bins, and the error on the colour depends on the magnitude (or rather magnitude bin) in question. For the sake of simplicity, they are determined only for $F110 - F160 = 0$ mag but have been shifted to the right hand side of the CMDs for visibility. Our brown dwarf candidate BD2 is marked with a red dot in the NIR CMDs. The violet triangle denotes the position of BD2 in the optical based on our old estimate (Dieball et al. 2016), the red cross denotes its position based on the comparison of aperture to PSF photometry, see Sect. 4 for more details.

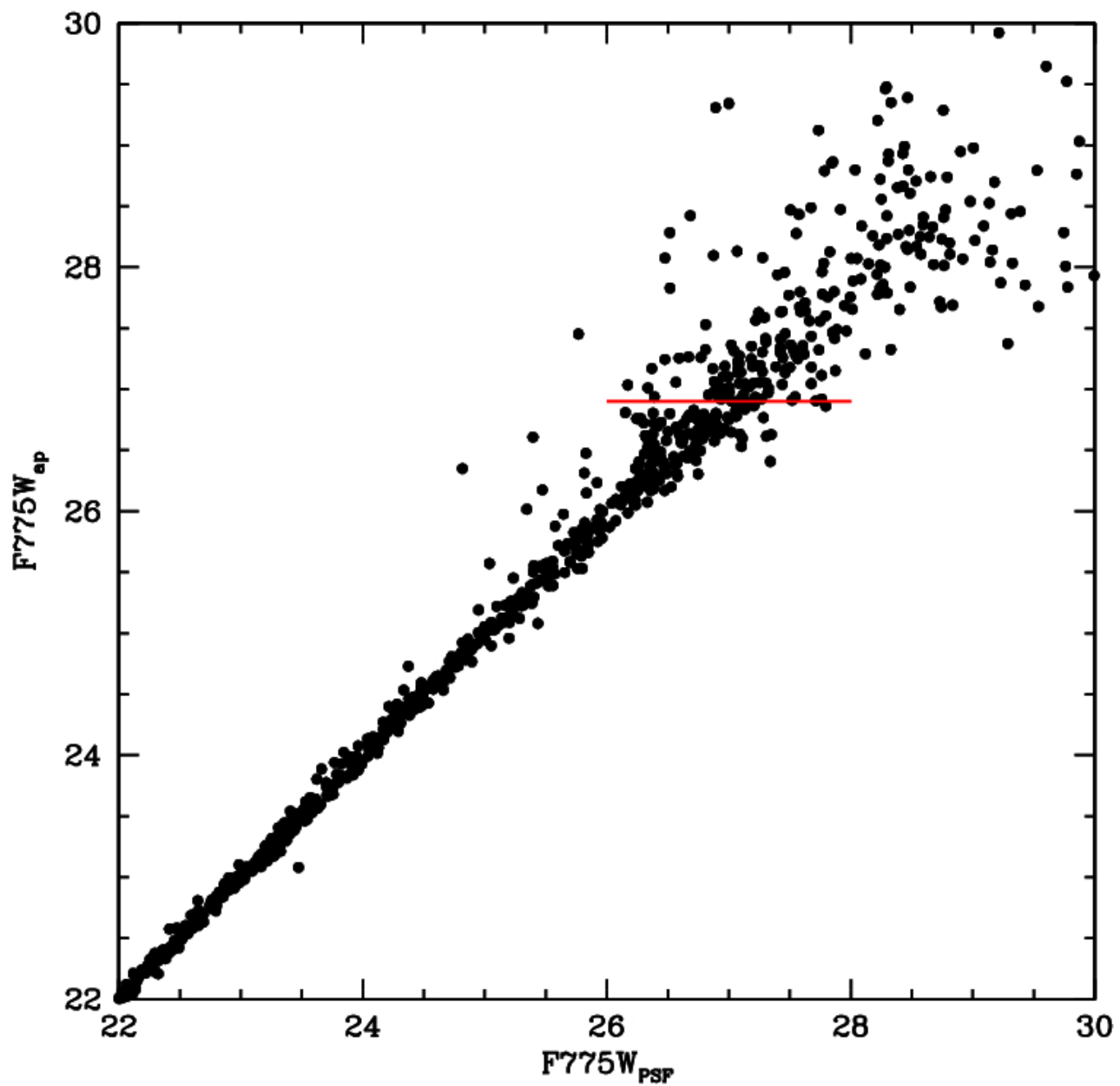


Figure 7. PSF photometry vs. aperture photometry for sources fainter than $F775W > 22$ mag. The spread between PSF and aperture photometry becomes larger for fainter source. The estimated magnitude for BD2 is marked with a red line.